Lattice-Oxygen Mobility across Inverse Oxide–Perovskite Interfaces for Low-Temperature CO Oxidation

Authors

Michael Tsz-Hin Lau[1], Karen Hoi-Yan Wong[2], Daniel Ka-Wai Chan[3*]

Affiliations

Department of Chemistry, The University of Hong Kong, Pokfulam Road, Hong Kong SAR, China

***Corresponding author:** kwchan@hku.hk

Abstract

Low-temperature CO oxidation over inverse oxide–perovskite catalysts is governed by the mobility of active oxygen species at the interface. In this work, inverse CuOx/perovskite catalysts were prepared by depositing dispersed CuOx domains on La-based perovskite supports and evaluated for CO oxidation between 80 and 180°C. H_2-TPR, O_2-TPD, in situ Raman spectroscopy, and $^{18}O_2$ isotopic exchange experiments were used to probe active-oxygen transport. The optimized catalyst achieved 90% CO conversion at 116°C, which was 48°C lower than that of the bare perovskite support. Isotope experiments showed that the lattice-oxygen exchange rate increased from 0.31 to 0.86 μmol g^{-1} s^{-1} after CuOx modification. In situ Raman spectra confirmed reversible formation of interfacial Cu–O–M species during CO oxidation. The results indicate that inverse oxide domains accelerate Mars–van Krevelen redox cycling by improving oxygen migration across the oxide–perovskite boundary.

Keywords: CO oxidation; inverse catalyst; CuOx; perovskite; lattice oxygen; oxygen mobility; Mars–van Krevelen mechanism

1. Introduction

Low-temperature CO oxidation is a key reaction in vehicle exhaust purification, industrial off-gas treatment, indoor air cleaning, and fuel-cell protection, where efficient CO removal is required at temperatures well below those used in conventional thermal catalysis. Noble metals such as Pt, Pd, Au, and Ru exhibit high intrinsic activity, but their high cost, limited availability, and sensitivity to operating conditions restrict their large-scale application. Transition-metal oxides provide an attractive alternative because their oxidation states, metal–oxygen bond strengths, and defect structures can be tuned over a wide range. Among them, CuO_x is particularly promising because the reversible Cu^+/Cu^{2+} redox cycle facilitates CO adsorption and oxygen activation, while the relatively low Cu–O bond energy favors oxygen participation at moderate temperatures [1,2]. However, isolated CuO_x particles tend to agglomerate during thermal treatment, and their oxygen transport can become kinetically limited when the particles grow or when highly reducible surface sites are depleted [3]. These limitations have shifted attention from

the properties of individual oxide phases toward the structure and dynamics of catalytic interfaces. Recent theoretical analysis of inverse ZrO_2/Cu catalysts has shown that an ensemble of structurally distinct interfacial sites can determine reaction pathways, catalytic reactivity, and deactivation behavior, emphasizing that catalytic performance may be governed by the local architecture of the interface rather than by the average properties of either component alone [4]. This interface-centered concept is highly relevant to oxide-based oxidation catalysts, in which the spatial arrangement of redox-active cations and mobile lattice oxygen can strongly affect reaction kinetics.

Perovskite oxides with the general formula ABO_3 provide a suitable platform for regulating these interfacial processes because their crystal structures tolerate substantial changes in cation composition, oxygen nonstoichiometry, and local lattice distortion. A-site deficiency, B-site substitution, and lattice strain can modify metal–oxygen covalency, oxygen-vacancy formation energy, and the mobility of lattice oxygen without destroying the basic perovskite framework [5,6]. These features are particularly important for CO oxidation, which over many transition-metal oxides proceeds through a Mars–van Krevelen mechanism. In this pathway, adsorbed CO reacts with surface or near-surface lattice oxygen to form CO_2, leaving behind an oxygen vacancy that is subsequently replenished by gas-phase O_2. Catalytic turnover therefore depends on the ability of the oxide to provide reactive oxygen, transport oxygen toward the reaction interface, and restore the lattice after oxygen removal. A catalyst with abundant surface oxygen may still exhibit poor low-temperature activity when bulk-to-surface oxygen migration or vacancy refilling is slow. Studies on $LaCoO_3$, $LaFeO_3$, and related La-based perovskites have demonstrated that cation substitution, nonstoichiometry, and controlled defect formation can lower reduction temperatures and enhance oxygen exchange and migration [7,8]. These findings indicate that oxygen mobility should be regarded as a dynamic kinetic parameter rather than simply as a static measure of surface oxygen concentration. Constructing a CuO_x–perovskite interface offers a complementary route for accelerating this oxygen-transfer process. When small CuO_x domains are dispersed on a reducible oxide surface, interfacial Cu–O–M linkages can be formed, where M represents a neighboring support cation such as Ce, Co, Mn, or Fe. Such linkages can redistribute electronic density between CuO_x and the support, stabilize mixed Cu oxidation states, alter the coordination environment of interfacial oxygen, and reduce the energy required for oxygen removal or migration. The resulting boundary can therefore function as a redox junction through which adsorbed CO, lattice oxygen, oxygen vacancies, and gas-phase O_2 are kinetically coupled. Enhanced CO oxidation activity has been reported for CuO_x/Co_3O_4, CuO_x/CeO_2, and Cu-containing ZnO-based systems relative to their corresponding individual oxide phases [9,10]. Similar behavior has been observed in $CuO/LaMnO_3$ composites, where Cu incorporation altered the surface concentrations of Cu^+, Mn^{4+}, and reactive oxygen species even though Cu did not substantially enter the perovskite lattice [11]. This observation suggests that the catalytic promotion originates primarily from interfacial reconstruction and electronic coupling rather than

from simple bulk substitution. Accordingly, the density, chemical identity, and reversibility of Cu–O–M boundary structures may be more important for low-temperature oxidation than the total Cu loading or Brunauer–Emmett–Teller surface area alone. Despite this progress, the relationship between interfacial structure and oxygen transport remains difficult to establish experimentally. Conventional X-ray diffraction can identify crystalline phases but is generally insensitive to highly dispersed or short-range interfacial structures. Ex situ X-ray photoelectron spectroscopy provides information on surface oxidation states, yet the oxidation state measured after cooling and air exposure may differ substantially from that present under reaction conditions. H_2 temperature-programmed reduction and O_2 temperature-programmed desorption are widely used to evaluate reducibility and oxygen release, but both techniques provide indirect descriptors and cannot independently determine the rate at which lattice oxygen moves across an oxide–oxide boundary during catalytic turnover. Surface oxygen ratios obtained from XPS are similarly influenced by hydroxylation, adsorbates, and sample handling. In situ and isotope-sensitive methods are therefore required to determine whether the apparent increase in reducibility is actually accompanied by faster oxygen exchange. In situ Raman spectroscopy is particularly useful for monitoring changes in metal–oxygen vibrations, lattice distortion, and the formation or disappearance of interfacial bonding motifs under controlled atmospheres [12,13]. Complementary $^{18}O_2$ isotope-exchange experiments can directly probe oxygen incorporation and lattice-oxygen replacement, providing quantitative information that cannot be obtained from reduction or desorption measurements alone [14,15]. Combining these methods creates a more direct route to connect a specific interfacial structure with its oxygen-transport function. A further challenge is that many reported comparisons between supported CuO_x catalysts and bare perovskites involve simultaneous variations in crystallite size, Cu dispersion, surface area, calcination history, defect concentration, and exposed crystal facets. These coupled variables make it difficult to determine whether improved CO conversion originates from the chemical interface itself or from unrelated changes in morphology and reducibility [16,17]. Quantitative isotope-exchange studies on dispersed CuO_x domains supported by La-based perovskites also remain scarce, particularly in the low-temperature region relevant to practical CO removal. Moreover, Cu–O–M configurations may be dynamically formed and removed as the catalyst undergoes reduction, oxidation, oxygen-vacancy generation, and vacancy refilling. A Cu–O–M structure detected in a fresh catalyst may therefore be absent under reaction conditions, while a catalytically important interfacial configuration generated during operation may disappear before conventional post-reaction characterization is performed. Resolving this issue requires characterization that follows the interface while the redox cycle is occurring and simultaneously measures the ability of oxygen to exchange through the lattice.

In this study, dispersed CuO_x domains are deposited on La-based perovskite supports to establish a well-defined oxide–perovskite boundary for low-temperature CO oxidation in the range of 80–180 °C. The work combines complementary measurements that probe different stages

of the oxygen-transfer process. H_2-TPR is used to evaluate changes in reduction behavior and the accessibility of redox-active oxygen, while O_2-TPD characterizes oxygen release and replenishment properties. In situ Raman spectroscopy is employed to follow the evolution of interfacial Cu–O–M bonding under relevant gas environments and to determine whether these structures are reversibly reconstructed during redox cycling. $^{18}O_2$ isotope-exchange experiments are further used to quantify lattice-oxygen exchange and provide a direct measure of oxygen transport across the CuO_x–perovskite interface. By correlating these measurements with CO conversion, the study seeks to establish a mechanistic relationship among reversible interfacial bonding, lattice-oxygen mobility, and catalytic turnover. Particular attention is given to whether the formation of Cu–O–M linkages facilitates oxygen removal from the perovskite lattice, promotes vacancy refilling by gas-phase O_2, and thereby accelerates the Mars–van Krevelen cycle at low temperature. Establishing this relationship would move the interpretation of CuO_x/perovskite catalysts beyond indirect descriptors such as reduction temperature or surface oxygen fraction and toward a dynamic description based on measurable oxygen-transfer kinetics. More broadly, the results are expected to clarify how oxide–oxide boundaries can be engineered as functional oxygen-transport pathways, providing a mechanistic basis for designing low-cost, noble-metal-free catalysts for efficient low-temperature oxidation reactions.

2. Materials and Methods

2.1 Catalyst Samples and Feed Gases

Nine catalyst samples were prepared. Three La-based perovskite supports, $LaMnO_3$, $LaFeO_3$, and $LaCoO_3$, were synthesized by a citrate sol–gel method. The required metal nitrates were dissolved in deionized water, and citric acid was added at a citric acid-to-metal molar ratio of 1.5. The solution was heated at 80°C until a gel formed. The gel was dried at 120°C and calcined at 700°C for 5 h. CuOx domains were then deposited on each support by deposition–precipitation, with a nominal Cu loading of 5 wt%. The resulting samples were denoted CuOx/$LaMnO_3$, CuOx/$LaFeO_3$, and CuOx/$LaCoO_3$. Bulk CuO, a CuO–$LaMnO_3$ physical mixture, and Cu-substituted $LaMn_{0.95}Cu_{0.05}O_3$ were prepared as reference samples. All catalysts were sieved to 180–250 μm before testing. CO, O_2, H_2, N_2, He, and $^{18}O_2$ with purities above 99.99% were used.

2.2 Reaction Design and Control Tests

CO oxidation was tested in a quartz fixed-bed reactor at atmospheric pressure. Each run used 100 mg of catalyst mixed with 300 mg of quartz sand. Before the reaction, the catalyst was treated in 10 vol% O_2/N_2 at 300°C for 1 h and then cooled to 80°C. The feed contained 1 vol% CO, 10 vol% O_2, and N_2 as the balance gas. The total flow rate was 100 mL min^{-1}, equal to a gas hourly space velocity of 60,000 mL g_cat^{-1} h^{-1}. The temperature was increased from 80 to 180°C at 2°C min^{-1}. The bare perovskites were tested to determine the effect of CuOx addition. Bulk CuO was tested to measure the activity of CuOx without a perovskite interface. The physical mixture was used to

distinguish simple contact from a formed CuOx–perovskite boundary. $LaMn_{0.95}Cu_{0.05}O_3$ was tested to compare surface CuOx domains with Cu located inside the perovskite lattice. Blank tests with quartz gave no measurable CO conversion.

2.3 Measurement Methods and Quality Control

Crystal phases were identified by X-ray diffraction with Cu Kα radiation. Specific surface areas were measured by N_2 adsorption at −196°C, and the Cu content was checked by inductively coupled plasma optical emission spectroscopy. H_2 temperature-programmed reduction was carried out from 50 to 700°C at 10°C min^{-1} in 10 vol% H_2/Ar. O_2 temperature-programmed desorption was measured after O_2 adsorption at 100°C, followed by heating to 700°C in He. In situ Raman spectra were collected from 100 to 1000 cm^{-1} during CO oxidation. The laser power was kept below 1 mW to limit local heating. For isotope exchange tests, the catalyst was first exposed to $^{16}O_2$ and then switched to $^{18}O_2$ at the selected temperature. The outlet isotope signals were measured by mass spectrometry. CO and CO_2 were also measured by online gas chromatography. Gas flow meters were calibrated before each test series. The catalyst-bed temperature was measured at the center of the bed and controlled within ±1°C. Each reaction test was repeated three times, and the carbon balance remained between 97% and 103%.

2.4 Data Processing and Model Equations

CO conversion was calculated from the inlet and outlet CO concentrations:

$$X_{CO}=\frac{C_{CO,in}-C_{CO,out}}{C_{CO,in}}\times 100\%$$

where $C_{CO,in}$ and $C_{CO,out}$ are the inlet and outlet CO concentrations, respectively. The lattice-oxygen exchange rate was calculated from the formation rate of ^{18}O-containing species:

$$r_{ex}=\frac{1}{m_{cat}}\frac{dn_{18O}}{dt}$$

where r_{ex} is the oxygen exchange rate, n_{18O} is the amount of exchanged ^{18}O, ttt is the exchange time, and m_{cat} is the catalyst mass. Raman peak areas were calculated after baseline correction. H_2-TPR and O_2-TPD peak areas were normalized by catalyst mass. The temperatures required for 50% and 90% CO conversion were obtained by interpolation from the light-off curves.

2.5 Kinetic and Statistical Analysis

Apparent activation energies were measured under differential conditions, with CO conversion kept below 15%. Reaction rates were recorded between 80 and 120°C and fitted with the Arrhenius equation. External and internal mass-transfer effects were checked by changing the total flow rate from 60 to 140 mL min^{-1} and the catalyst particle size from 100–180 to 250–425 μm. No clear rate change was found within the selected ranges. Pearson correlation analysis was used to compare CO oxidation rates with H_2 consumption, oxygen desorption, Raman peak

changes, and lattice-oxygen exchange rates. Differences among catalyst samples were tested by one-way analysis of variance followed by Tukey's test. Differences were considered significant at $p<0.05$. Results are reported as the mean ± standard deviation of three independent tests.

3. Results and Discussion

3.1 CO Oxidation Activity of the Inverse Catalysts

CuOx loading improved the low-temperature activity of all three perovskite supports. The extent of improvement depended on the B-site metal. Bare $LaMnO_3$ reached 90% CO conversion at 164°C. After CuOx loading, the T_{90} value decreased to 116°C, which was 48°C lower than that of the bare support. The T_{90} values of CuOx/$LaCoO_3$ and CuOx/$LaFeO_3$ were 128 and 137°C, respectively. Bulk CuO required 152°C, while the CuO–$LaMnO_3$ physical mixture reached 90% conversion at 143°C. $LaMn_{0.95}Cu_{0.05}O_3$ was less active than CuOx/$LaMnO_3$, although both samples had the same nominal Cu content. This result shows that CuOx domains at the outer interface were more active than Cu incorporated into the perovskite lattice. The activity curves and control results are shown in Fig. 1. The physical mixture gave only a small improvement because simple contact between the two phases did not form enough Cu–O–Mn sites [18,19]. Jiao et al. (2026) also found that supported Cu species improved CO oxidation, but activity did not increase directly with Cu loading. Their results were related to the number and reduction behavior of surface Cu sites. The present results further show that a formed CuOx–perovskite interface is more active than simple phase contact or lattice-substituted Cu.

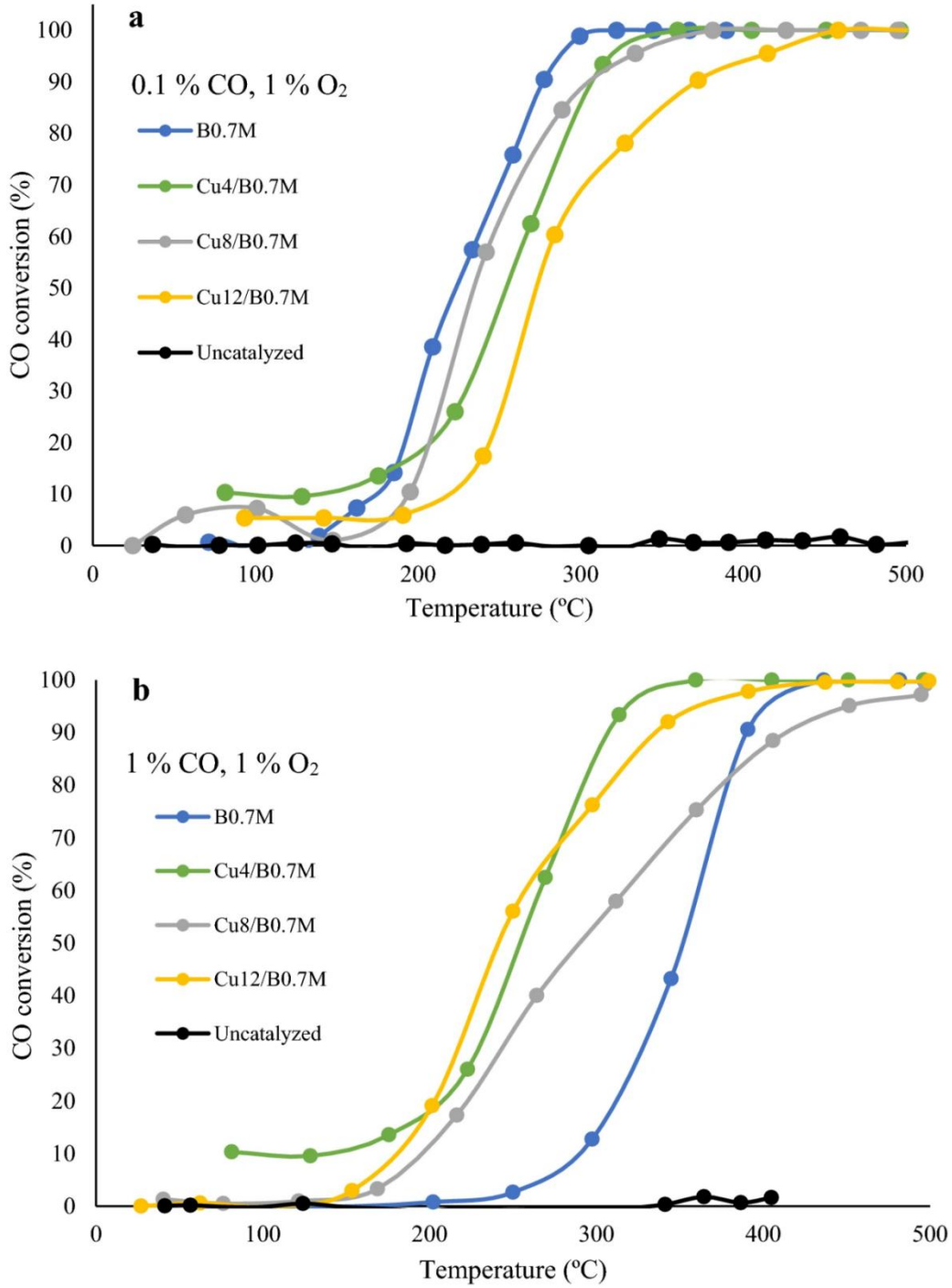

Fig. 1. CO conversion and light-off temperatures of the CuOx/perovskite catalysts and reference samples.

3.2 Reduction Behavior and Oxygen Release

The H_2-TPR results showed that CuOx lowered the reduction temperature of the perovskite surface. $LaMnO_3$ had a broad reduction peak near 315°C. CuOx/$LaMnO_3$ showed a new low-temperature peak at about 198°C. This peak was assigned to CuOx species in close contact with Mn–O units. The main reduction peak of the perovskite also shifted to a lower temperature. This change shows that CuOx weakened nearby Mn–O bonds. CuOx/$LaCoO_3$ showed a smaller

shift, while CuOx/$LaFeO_3$ showed only a limited change. The O_2-TPD results followed the same order. CuOx/$LaMnO_3$ released more oxygen below 300°C than the other samples. The bare supports mainly released oxygen at higher temperatures. The low-temperature oxygen amount increased from 0.18 mmol g^{-1} for $LaMnO_3$ to 0.47 mmol g^{-1} after CuOx loading. These results show that the interface increased the amount of available oxygen and lowered its release temperature. Wu et al. (2026) also reported that changes in Cu–O and Mn–O bonding improved lattice-oxygen release in Cu-containing perovskites. Their results linked oxygen mobility with higher CO oxidation activity. However, temperature-programmed tests do not directly show whether the released oxygen takes part in the reaction. Isotope exchange and Raman measurements were therefore used to examine oxygen transport under working conditions [20,21].

3.3 Lattice-Oxygen Exchange and Interfacial Bond Changes

The $^{18}O_2$ switching tests gave direct evidence of faster oxygen transport after CuOx loading. The lattice-oxygen exchange rate increased from 0.31 μmol g^{-1} s^{-1} for $LaMnO_3$ to 0.86 μmol g^{-1} s^{-1} for CuOx/$LaMnO_3$. CuOx/$LaCoO_3$ and CuOx/$LaFeO_3$ gave lower rates of 0.69 and 0.55 μmol g^{-1} s^{-1}, respectively. The physical mixture showed an exchange rate of only 0.43 μmol g^{-1} s^{-1}. These results show that close interfacial contact was required for fast oxygen movement. The in situ Raman spectra also changed after the CO/O_2 feed was introduced. The CuOx band became weaker, while a broad Cu–O–M band increased. The original spectrum returned after CO was removed. This reversible change shows that the interfacial bonds formed and disappeared during the redox cycle. The isotope signals, temperature-programmed profiles, and Raman spectra are shown in Fig. 2. The relation between the Raman signal and the ^{18}O exchange rate suggests that Cu–O–M sites served as oxygen-transfer paths. Cattelan et al. (2025) reported that interface-driven lattice changes activated surface oxygen during low-temperature CO oxidation over Pt/TiO_2. Their operando results showed that both lattice oxygen and adsorbed oxygen took part in the reaction [22,23]. The present results show a similar oxygen-transfer process in a noble-metal-free CuOx/perovskite system.

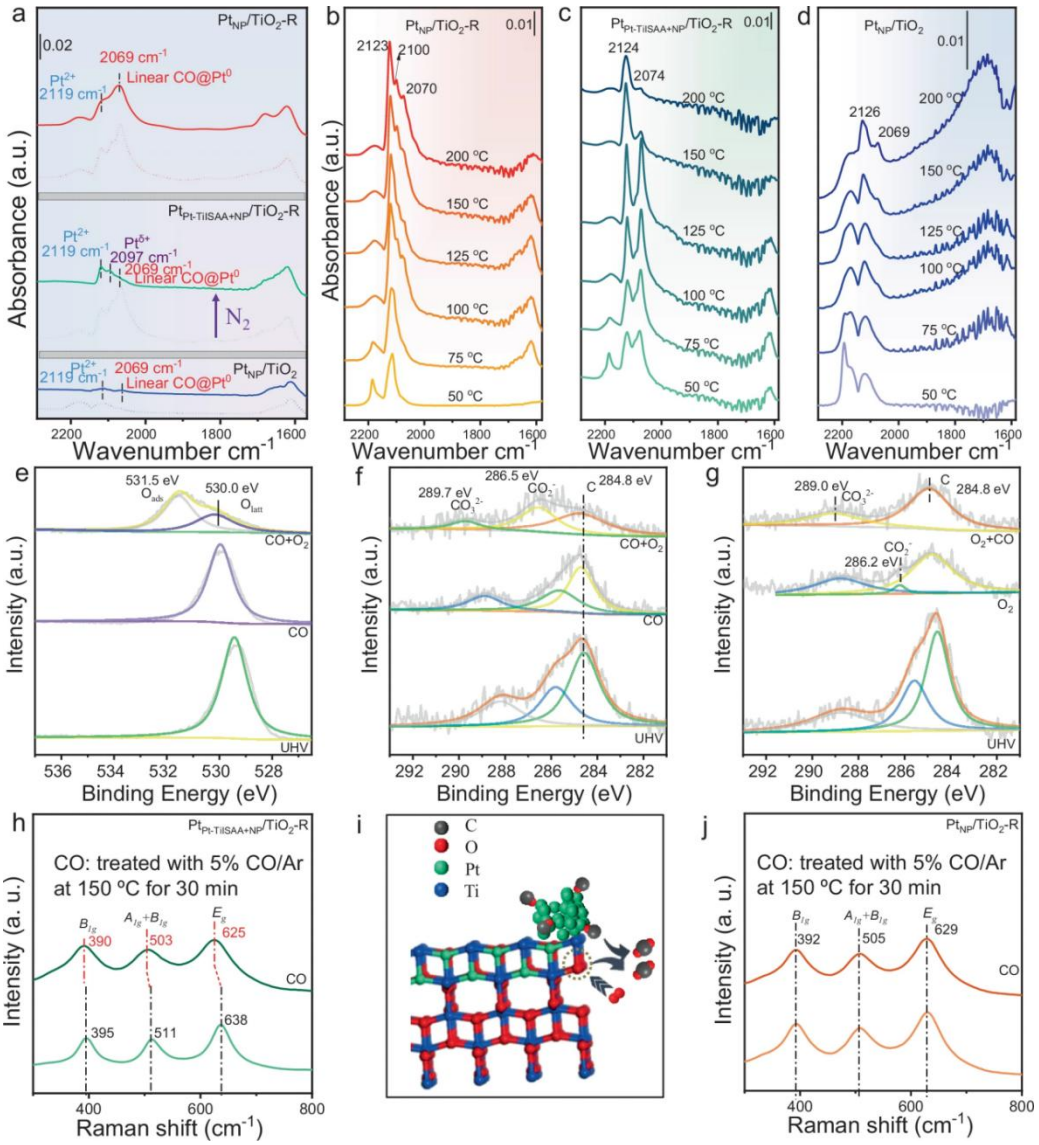

Fig. 2. Reduction behavior, oxygen release, lattice-oxygen exchange, and Raman spectra of the CuOx/perovskite catalysts.

3.4 Relation between Oxygen Mobility and CO Oxidation

The CO oxidation rate showed only a weak relation with BET surface area. The corresponding R^2 value was 0.32. In contrast, the reaction rate was closely related to the ^{18}O exchange rate, with R^2=0.94. A similar relation was found between activity and the reversible Raman signal assigned to Cu–O–M bonds. The apparent activation energy decreased from 63.1 kJ mol⁻¹ for $LaMnO_3$ to 41.7 kJ mol⁻¹ for CuOx/$LaMnO_3$. The physical mixture gave an intermediate value of 54.6 kJ mol⁻¹. These results support a Mars–van Krevelen route. CO removes oxygen near the interface, and gas-phase O_2 then restores the reduced sites through lattice-oxygen transport. CuOx supports this cycle by providing CO adsorption sites and lowering the barrier for oxygen migration from the perovskite. $LaMnO_3$ gave the best result because its Mn–O network could exchange oxygen more easily after contact with CuOx. The $LaFeO_3$ interface was less

active because its lattice oxygen was harder to remove under the tested conditions. Cano-Blanco et al. (2025) also found that CO oxidation depended on surface Cu species and support oxygen vacancies rather than on Cu loading alone. Hadjiivanov et al. (2026) linked high activity with easy reduction, oxygen vacancies, and mobile lattice oxygen. The present study adds direct isotope evidence and identifies the reversible Cu–O–M boundary as the main oxygen-transfer region [24].

4. Conclusion

CuOx loading improved low-temperature CO oxidation by increasing oxygen movement across the oxide–perovskite interface. The best catalyst reached 90% CO conversion at 116°C, which was 48°C lower than the bare perovskite support. The lattice-oxygen exchange rate increased from 0.31 to 0.86 μmol g^{-1} s^{-1} after CuOx loading. In situ Raman spectra showed that Cu–O–M bonds formed and changed reversibly during the reaction. These interfacial sites supported faster lattice-oxygen transfer and promoted the Mars–van Krevelen cycle. This work links oxygen exchange, interfacial bond changes, and CO oxidation activity under reaction conditions. The results may help improve noble-metal-free catalysts for vehicle exhaust treatment, indoor air cleaning, and low-temperature gas purification. However, only a small group of La-based perovskites was tested at laboratory scale. Longer stability tests, wider Cu loading ranges, and feeds containing water or sulfur compounds are needed. Atomic-scale measurements are also required to confirm the structure and lifetime of the active interface under practical conditions.

References

1. Gu, X. (2026). Identifying Causal Effects and Analyzing Heterogeneity of User Growth Interventions on Digital Platforms: Evidence from Large-Scale Behavioral Data. Available at SSRN 6809181.

2. Hassan, A. A., Farrag, M., Gabr, R. M., & Said, M. I. (2025). Enhanced Dehydrogenation of 2-Propanol via Surface Synergism of CuO@ Nanostructured Ceria Derived from Modified Ce-UiO-66. Catalysis Letters, 155(10), 334.

3. You, S. (2026). Verifiable Audit Mechanisms in AI Compliance Automation: Scalability. Available at SSRN 6547458.

4. Yang, Z., Alexandrova, A. N., & Sautet, P. (2026). Modeling CO2 Hydrogenation to Methanol on an Ensemble of Inverse ZrO2 on Cu Catalytic Sites: Mechanism, Reactivity, and Deactivation. Angewandte Chemie, e5448247.

5. Christy, M., Choi, S., Kwon, J., Jeong, J., Paik, U., & Song, T. (2025). The perfect imperfections of perovskite oxide catalysts in the aspect of defect equilibria. Small Science, 5(1), 2400386.

6. Jiao, Y., Shi, T., Zhao, B., & Wang, A. (2026). The Impact of VR Sketching Simulations on the Assessment of Scale and Site Suitability in Public Art Spaces.

7. Diaz, D., Arias, D., Díaz de León, J. N., Dongil, A. B., Martínez-Quintana, L., Escalona, N., ... & Sepulveda, C. (2026). Effect of Partial Co and Fe Substitution on LaFeO3@ C, LaCoO3@ C Catalysts in the Oxidation of Furfural. Reactions, 7(2), 28.
8. Liang, S., Zhang, X., Du, Y., & Chen, W. (2026). Supply Network Restructuring and Capacity Ramp-Up Limits in the Localized Expansion of High-Performance Computing Equipment Production. Available at SSRN 7339738.
9. Bao, Y., & Wang, H. (2026). Edge-to-Cloud Infrastructure Continuum: A Unified Framework for Optimizing Industrial IoT Systems. Available at SSRN 7185578.
10. Hussain, A., Hussain, M., Khan, M. T., Park, D., Ud Din, H., Myoung, N., ... & Son, Y. (2026). Electro-Optical Correlation of Charge-Transfer Kinetics in Composition-Tuned Wurtzite Oxide Anodes for Sodium-Ion Storage. Materials, 19(17), 3643.
11. Chen, F., Liang, H., Li, S., Yue, L., & Xu, P. (2025). Design of Domestic Chip Scheduling Architecture for Smart Grid Based on Edge Collaboration.
12. Kumar, N., Najimu, M. O., Cho, Y. J., Gilliard-AbdulAziz, K. L., Nikolla, E., Wu, Z., & Wachs, I. E. (2025). Probing surface/bulk structural chemistry of key components of solid oxide electrochemical cells with in situ/operando Raman spectroscopy. Chemical Reviews, 125(18), 8921.
13. Liang, R., Feifan, F. N. U., Liang, Y., & Ye, Z. (2025). Emotion-Aware Interface Adaptation in Mobile Applications Based on Color Psychology and Multimodal User State Recognition. Frontiers in Artificial Intelligence Research, 2(1), 51-57.
14. Hadjiivanov, K., Panayotov, D., & Mihaylov, M. (2026). Isotopic labeling in IR spectroscopy of surface species: A powerful approach to advanced surface investigations. Catalysts, 16(1), 57.
15. Du, Y. (2025). Research on Digital Quality Traceability System for Temperature-Controlled Supply Chain of Foreign Trade Wine Driven by Blockchain and IoT. Business and Social Sciences Proceedings, 4, 57-65.
16. Nunes, L. J. (2026). Controlling oxygen in biomass-to-energy chemistry: catalytic pathways from lignocellulosic oxygenates to renewable fuels and energy carriers. Biofuels, 1-21.
17. Jiao, Y., Zhao, B., Wang, A., & Shi, T. (2026). Construction and Empirical Study of a Modularized Teaching System for Art Courses Based on a Unified Training Pathway.
18. Schichtl, Z. G., Carvalho, O. Q., Tan, J., Saund, S. S., Ghoshal, D., Wilder, L. M., ... & Greenaway, A. L. (2025). Chemistry of materials underpinning photoelectrochemical solar fuel production. Chemical Reviews, 125(10), 4768.
19. Yang, J. (2026). Stage-Coupled Computational Framework for Stratified Accessibility and Equity Analysis in Community-Based Elderly Care Services.
20. Feldl, J., Gillen, R., Maultzsch, J., Papadogianni, A., Kler, J., Galazka, Z., ... & Ramsteiner, M. (2025). Unravelling the oxygen influence in cubic bixbyite In2O3 on Raman active phonon modes by isotope studies. Journal of Materials Chemistry C, 13(47), 23545-23553.

21. Wu, J., Wu, D., Zhang, J., & Peng, Y. (2026). Generative AI Feedback in Junior High School Artistic Creation Evaluation. Available at SSRN 7244838.
22. Cattelan, M., Yang, J., Cielo, L., Nappini, S., Carlotto, S., Nalesso, M., ... & Agnoli, S. (2025). Operando Exploration of CoAl-LDH: Transformations Driving Alkaline Oxygen Evolution Reaction. Small, 21(19), 2412351.
23. Bao, Y., Qiu, Y., & Wang, H. (2026, May). Unified Identity Layer for Hyperscale Ecosystems: A Framework for Cross-Platform User Attribution and Experimentation. In 2026 6th International Conference on Machine Learning and Intelligent Systems Engineering (MLISE) (pp. 540-543). IEEE.
24. Cano-Blanco, D. C., Fischer, J. W., Buttignol, F., Alxneit, I., Jeschke, G., Krocher, O., & Ferri, D. (2025). Monomeric Fe in six-membered rings at work: operando spectroscopy of nitrous oxide activation and decomposition over Fe-exchanged zeolites. ACS Catalysis, 15(17), 15579-15595.